2017

UNDERDETERMINED SIGNAL REPRESENTATION VIA LINEAR PROJECTIONS USING BINARY SPARSE MATRICES- SIGNAL COMPRESSION

Stefan Leitner
ls3130@siu.edu

Recommended Citation

Leitner, Stefan. "UNDERDETERMINED SIGNAL REPRESENTATION VIA LINEAR PROJECTIONS USING BINARY SPARSE MATRICES- SIGNAL COMPRESSION." (Jan 2017).

UNDERDETERMINED SIGNAL REPRESENTATION VIA LINEAR PROJECTIONS
USING BINARY SPARSE MATRICES- SIGNAL COMPRESSION

by

Leitner Stefan

B.S., Management Center Innsbruck, 2013
M.Sc., Southern Illinois University, 2016

A Research Paper
Submitted in Partial Fulfillment of the Requirements for the
Master of Science

Department of Mathematics
in the Graduate School
Southern Illinois University Carbondale
May 2017

RESEARCH PAPER APPROVAL

UNDERDETERMINED SIGNAL REPRESENTATION VIA LINEAR PROJECTIONS
USING BINARY SPARSE MATRICES- SIGNAL COMPRESSION
By

Leitner Stefan

A Research Paper Submitted in Partial

Fulfillment of the Requirements

for the Degree of

Master of Science

in the field of Mathematics

Approved by:

Dr. Kathleen Pericak Spector, Chair

Graduate School
Southern Illinois University Carbondale
March 10, 2017

AN ABSTRACT OF THE RESEARCH PAPER OF

LEITNER STEFAN, for the Master of Science degree in MATHEMATICS, presented on MARCH 10, 2017, at Southern Illinois University Carbondale.

TITLE: UNDERDETERMINED SIGNAL REPRESENTATION VIA LINEAR PROJECTIONS USING BINARY SPARSE MATRICES- SIGNAL COMPRESSION

MAJOR PROFESSOR: Dr. Kathleen Pericak Spector

This paper presents and studies analytically a new compressive sensing (CS) approach with the aim of bringing this technique closer to successful commercialization in image sensor circuits. Unlike existing CS techniques that use random measurement matrices (RMM) to encode a signal given in form of a vector of discrete samples, the proposed technique utilizes carefully chosen custom measurement matrices. In CS measurement operation, RMM are often used to achieve small coherence between the measurement matrix and the sparse representation bases. However, when applied in practice, RMM based CS designs typically lead to complicated hardware design and thus have a large circuit overhead to obtain random summations. The proposed custom measurement matrix achieves about the same level of incoherence as the RMMs, but results in a dramatically simplified CS measurement circuit, improving both energy efficiency and circuit scalability, and thus the attractiveness of this technique for industrial commercialization. The proposed method is evaluated analytically in terms of Peak Signal to Noise Ratio (PSNR), a measure for the quality of the reconstructed compared to the original signal. Matlab simulations are also conducted to evaluate the effectiveness of the proposed technique, and to compare simulated and estimated PSNRs. Finally, the proposed technique is extended to two-dimensional projections with the aim of further improving signal quality, in particular with high compression rates. A

newly formulated minimization problem is proposed to combine the projections in both

dimensions to a single optimization problem.

PREFACE

Writing this paper about Compressive Sensing is motivated by the authors prior experience in this field. While pursuing a Master of Science degree in Electrical and Computer Engineering, research has been carried out on the topic of Compressive Sensing related to the process of capturing images in camera devices. During this period, a new image compression technique has been found and experimentally evaluated. Results suggest that the newly found technique is very promising, as it has significant advantages in terms of simplicity and thus power consumption of circuits carrying out the task of image compression. The quality of reconstructed images has also been found to be superior compared to conventional techniques. Results have been, or are in the process to be, published in scientific conference [10] and journal papers, and a provisional patent application has been filed.

The aim of this paper is to study the proposed technique analytically. Due to the complexity of the underlying topic and the time available to write this paper it is not possible to provide a rigorous proof of the validity of the new measurement technique. The analytic discussion in this paper merely intends to give more insight into this method, and to explain intuitively why the proposed technique might be the better choice when performing image compression.

The technique discussed in this paper is applicable in many different fields, and on signals of any kind, as long as certain properties are satisfied. However, since writing this paper is motivated by prior experience in compressive acquisition of image data, the concept of this technique as well as the topic in general will be introduced and studied in the context of compressive image acquisition.

TABLE OF CONTENTS

LIST OF TABLES

LIST OF FIGURES

INTRODUCTION

Image sensors have been used in a wide range of applications such as consumer electronics, medical diagnosis instruments, robotics, defense and reconnaissance equipment. Due to the rich information provided by images and videos, image sensors are also widespread in Internet of Things (IoT) applications, which is currently a booming field. Driven by these applications, the image sensor industry has been experiencing an explosive growth and its market revenue is expected to be over $15B in 2020 [1]. Along this impressive development trend, there are increasing demands for high resolution and high frame rate image sensors to attain better user experience or to provide more detailed images for industrial, scientific and military applications.

IoT devices, but image sensors in general, often have very stringent power budgets, limited computation and communication capabilities. For example, such devices are extremely desirable for hand-held or wearable gadgets, and might be mandatory in swallow-able medical devices due to power and heat dissipation constraints. On the other hand, image sensors tend to be power hungry and often generate large volumes of raw data for being processed, stored or transmitted. Unfortunately, the enhancement of image sensor resolution and frame rate also undesirably increases the power consumption of such sensors, which limits the suitability of such sensors in many applications. For example, a high resolution image sensor may not be used in an endoscopic instrument due to the heat problem associated with the high power consumption of the image sensor. Additional examples can be easily found in many other application domains, such as wearable devices, Internet of Things (IoT), and aerospace applications. Circuit techniques and fabrication processes have been

aggressively exploited to reduce the image sensor power consumption over the past few decades [2-3]. However, with the rapid increase of image sensor resolutions (e.g. from past VGA to current 1080p and near future 4K ultra HD), continuously reducing power consumption with these traditional approaches alone will become more challenging since the number of pixels that have to be captured and digitized is exponentially growing.

Recently, compressive sensing (CS) emerged as a promising technique to accomplish low power image acquisition [4-5]. Instead of digitizing every pixel, CS image sensors digitize only a small set of random summations of the pixels. Therefore, the number of measurements can be significantly smaller than the number of pixels. From this small set of measurement data, the image can still be reconstructed with high fidelity via CS techniques. It has the potential to dramatically reduce the amount of data to be digitized and subsequently transmitted. Since the analog to digital conversion (ADC) as well as the data transmission consumes a significant portion of the image sensor power, CS techniques hold great promise for dramatically reducing the power consumption at the image sensing end. Motivated by such potentials, several CS image sensor circuits were developed in the past few years. Despite the fact that these implementations clearly demonstrated the feasibility and power saving advantages, CS techniques have not yet been widely used in CMOS image sensor circuits. One of the major hurdles toward the wide acceptance of CS techniques in CMOS image sensor design is the very complex circuit structure and thus the difficulty to scale the existing CS image measurement circuits to high resolution image sensors.

In this paper a modified image compression approach is presented which leads to energy and hardware efficient CS measurement circuits for CMOS image sensors. The proposed method targets image sensors capturing natural images. Statistical data show that the vast majority of the signal power of natural images is described by low frequency (or low index) coefficients in their sparse representations with properly selected sparse basis [6]. In plain terms, it means the average variance of the pixel power among neighboring pixels is small. Taking advantage of this property, unlike the existing CS image sensors that use random measurement matrices (RMM) in CS measurement operation, the proposed measurement technique utilizes a carefully chosen custom measurement matrix. Typically, RMM are selected to achieve small coherence between the measurement matrix and the spare base matrices used in CS operation [7]. However, the implementation of the RMM based CS circuits not only requires large linear feedback shift registers (LFSR) but also leads to complex circuit structures to perform pixel summation. The proposed custom measurement matrices achieve about the same level of incoherence but result in a dramatically simplified CS measurement circuit. This improves the energy efficiency as well as the scalability of CS image sensor circuits, and makes the CS technique, in general, more appealing to the industry.

The aim of this paper is to give an introduction to compressive sensing theory and to provide closed form expressions to compute lower bounds for the minimum signal quality of the compressed and reconstructed signals (upper bounds of the error between original and reconstructed data), based on the assumption that the signals satisfy the sparseness and low variance properties, whose definitions are given in a later section. Matlab simulations are conducted to evaluate the derived expressions, and the

effectiveness of the proposed technique. Results indicate that good quality images can

be obtained with the proposed measurement matrices, and that the derived minimum

signal quality bounds are valid.

THEORY OF COMPRESSIVE SENSING

The mathematical framework of CS was developed about a decade ago [4, 5] and shortly after that CS techniques were applied in various fields including image sensing, image denoising, image de-blurring, sub-Niquist sensing of signals, radar, ultra-wide-band communication, low-power sensors, etc [11]. The most appealing feature of CS techniques is the ability to recover a sparse signal x with N data points from less than N measurements. This idea can be used to reduce hardware size, relax circuit performance requirements, minimize system operation, or reduce power consumption at the sensing end. To take advantage of the CS concept, the signal under consideration must be sparse. Sparsity is defined as follows. Assume x is a one dimensional vector with N elements and Ψ is a matrix of dimension $N \times N$, whose column vectors ψ_i form an orthonormal bases. The projection of x on domain Ψ is given by coordinate vector $[s]_\Psi$, such that $x = \sum_1^N \psi_i s_i$; $(x = \Psi \cdot [s]_\Psi)$, where s_i is the ith element of $[s]_\Psi$. If the number of non-zero (or significant) terms in $[s]_\Psi$ is significantly smaller than N (for example, if less than 10% of the coefficients have a magnitude larger than 1% of the magnitude of the dominant component), signal x is called sparse with respect to basis Ψ. A vector is defined to be k-sparse if it has at most k non-zero or significant elements.

In real applications, many signals are not sparse in their original form but become sparse after being projected into another domain; which can be applied to CS techniques in fields like image sensing. In the typical operation of CS image sensors, the pixel values are not directly measured and digitized. Instead, a set of random summations of pixel values are measured. For convenience, the pixel data is expressed in column

vector x of length N for a $p \times q$ dimensional pixel array, where $N = p \times q$. The measured

signal, denoted by y, can be expressed as $y = \Phi \cdot x$. Φ is referred to as the

measurement matrix with dimension $M \times N$, whose rows are denoted by φ_i. If $M < N$, y

has less data points than x and hence less data needs to be measured and processed

when CS techniques are applied. The ratio of N over M is referred to as the compression

rate R.

To recover signal x from y, the system requires prior knowledge of Ψ and Φ. With

the measurement data y it solves for $[s]_\Psi$ from $y = \Phi \cdot \Psi \cdot [s]_\Psi$. Since $M < N$, this is an

underdetermined system and its solution is not unique. Here, the signal sparsity comes

to the rescue and it has been proven that the sparsest solution, the one that contains the

least number of nonzero terms, has a very high probability to be a close approximation to

the correct solution [5]. Once the values of $[s]_\Psi$ are obtained, signal x can be easily

reconstructed by the projection relation $x = \Psi \cdot [s]_\Psi$.

Several conditions for selecting matrix Φ to guarantee the recovery of x have

been derived by experts in mathematical fields, such as constraints in terms of spark,

coherence, Null space, restricted isometry property (RIP), etc. Meanwhile, various

methods to recover x have also been developed, including adaptive binary search, l_1

minimization (or basis pursuit), greedy pursuits, etc. Among them, the RIP condition and

the basis pursuit recovery method are frequently used in CS related applications. The

RIP was originally defined as follows [5]: Matrix Φ obeys the RIP with constant δ_k if:

$$(1 - \delta_k)\big||x|\big|_2^2 \leq \big||\Phi \cdot x|\big|_2^2 \leq (1 + \delta_k)\big||x|\big|_2^2 \qquad (1)$$

for all k-sparse vectors x, $|| \; ||_2$ denoting the standard l_2-norm on $\Re^d$. To be able to

recover vector x, δ_k needs to be smaller than certain thresholds. Intuitively, δ_k indicates

how well the linear observations, $\Phi \cdot x$, preserve the energy of the signal vector x. The smaller δ_k is, the better the signal energy is preserved. Later, the RIP is generalized with condition [8]: $(1 - \delta_k)||x||_p \le ||\Phi \cdot x||_p \le (1 + \delta_k)||x||_p$. It shows that RIP with $p = 1$, denoted as RIP-1, can also be used to select Φ to guarantee the recovery of x. Note that these conditions are typically sufficient, but not necessary. For example, a matrix that satisfies RIP-1 guarantees signal recovery, but may not satisfy the original RIP-2 condition, and vice versa. Thus neither of the conditions is stronger than the other.

The mathematical theory behind the CS operation also indicates that the sparsest solution can be obtained by solving a convex minimization problem formulated as follows:

$$min\big|\big|[s]_\Psi\big|\big|_{l_1}, subj.\ to\ y = \Phi \cdot \Psi \cdot [s]_\Psi \tag{2}$$

To recover signal x with a high confidence level, the above approach also requires:

1) the measurement size M meets the lower bound requirement: $M \ge O\left(k \cdot log\left(\frac{N}{k}\right)\right)$, where k is the number of non-zero or significant terms in vector $[s]_\Psi$ (sparsity of $[s]_\Psi$);

2) the measurement matrix Φ and sparse basis Ψ are incoherent. This means the coherence measure μ given below should be small.

$$\mu(\Phi, \Psi) = \sqrt{N} \cdot \max_{1 \le i \le M; 1 \le j \le N} |\langle \varphi_i, \psi_j \rangle| \tag{3}$$

It has been shown that $\mu(\Phi, \Psi) \in [1, \sqrt{N}]$ for any normalized matrices Φ and Ψ [7]. Finally, it is observed that random measurement matrices are largely incoherent to many sparse bases used in CS operations [7], which is the reason why random measurement matrices are often used in the existing CS image sensor implementations.

For the completeness of discussion, the Sparse Representation- Based Super-Resolution (SR) technique [11] should also be mentioned. The SR technique aims to recover a high-resolution image from one or a multiple of low-resolution images. The low quality signals treated in SR stem from a high resolution image, whose signal attenuation is due to non-ideal low-pass filtering and/or decimation filtering effects. Unlike what occurs in CS, these signal attenuations are undesired, and not part of a prior compression process. The projection operator in SR (equivalent of Φ in CS) is therefore unknown. Still, CS theory can be applied to SR by modeling the non-ideal image capturing and processing effects via a projection operator L. Thus the low-resolution image is viewed as if it were obtained via a dimension diminishing map L from the high resolution image, with the difference that the projection operator cannot be chosen, but is rather dependent on many artificial circumstances. Unlike random matrices in CS, the RS operator is frequency discriminative, i.e., low frequency content in the signal is preserved well, while high frequency components are largely attenuated [11]. Thus unlike in CS, the quality of the reconstructed image is a function of the frequency spectrum of the original signal. The proposed technique presented in the next section belongs to the field of CS, but has similarities with RS in terms of the frequency discriminative behavior of the projection operator. As explained below however, attenuation of high frequency signal content is not performance critical for the overwhelming majority of natural images.

PROPOSED COMPRESSION METHOD

A. Introduction to the Proposed CS Technique

Unlike the existing CS image sensor circuits that perform random summations for variable sets of samples of x, the proposed method follows regular patterns to sum neighboring pixels within the same column or row of the two-dimensional image array. It can be explained with the following example. Without losing generality, assume the CS measurement is conducted for a column vector containing 256 samples and the compression rate R is 4. R is defined as the ratio of the number of pixels over the number of CS measurements. Thus, 64 CS measurements are to be generated, which are denoted by $\mathbb{S}_1$, $\mathbb{S}_2$, $\cdots \mathbb{S}_{64}$. To generate a single CS measurement, six neighboring samples are added together and there is an overlap of two samples between two neighboring summation groups. The CS measurement operations are illustrated in Fig. 1. Note that the vertical bars in the figure represent the same sample column and the groups of six samples in the shaded regions are added together to produce the 64 CS measurements. The starting and ending pixel positions of each summation group are listed on the left side of the shaded regions. For example, in the first CS measurement, the outputs of samples $1 \sim 3$ and $254 \sim 256$ are added together; in the second CS measurement, the outputs of samples $2 \sim 7$ are added. Thereafter, the position of the measurement group is moved by 4 samples to start the next CS measurement.
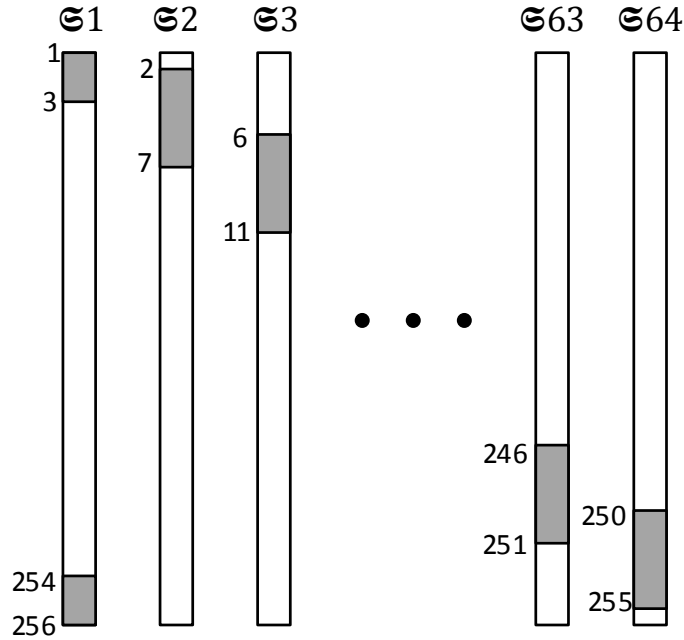
Fig. 1. Example pixel access pattern in CS measurement operation

The sample summations can, in general, be described by the following equations:

$$\mathfrak{S}_1^m = \sum_{i=m\cdot p+1}^{m\cdot p+3} x(i) + \sum_{i=(m+1)\cdot p-2}^{(m+1)\cdot p} x(i)$$

$$\tag{4}$$

$$\mathfrak{S}_k^m = \sum_{i=m\cdot p+4\cdot k-6}^{m\cdot p+4\cdot k-1} x(i), \qquad 1 < k \le 64$$

In the above equations, letter m indicates for which pixel column the CS measurement is performed, and $0 \le m \le q-1$, for a $p \times q$ dimensional image array (In the example, p is chosen as 256, with measurement supports of 6 samples each). In general, to generate M CS measurements for a pixel array containing N pixels, the size of summation groups should be $\frac{N}{M} + OL$, where OL represents the number of overlapping samples between two neighboring summation groups. As a guideline, OL is preferred to be selected as $\frac{R}{2}$, if

possible. For given N, M, and *OL* values, the entries of measurement matrix ϕ can be determined using:

$$\phi(i,j) = \begin{cases} 1 & if\ 1 + \dfrac{(i-1) \cdot N}{M} \leq j \leq \dfrac{i \cdot N}{M} + OL \\ 0 & otherwise \end{cases} \tag{5}$$

for $1 < i < M$. For $i = 1, M$ (the first and last row respectively), the pattern needs to be slightly adjusted to meet the image size constraint, since the dimension of the frame may not be a multiple of $\frac{N}{M}$.

B.   Justification of Proposed CS Measurement Method

As discussed earlier, signals must be sparse with respect to a sparse basis to be able to take advantage of CS techniques. Image signals are generally sparse with respect to an inverse discrete cosine transform (IDCT) basis. The vectors in IDCT correspond to samples of the cosine function with variable frequency starting from DC, which are given as:

$$\Psi(k,j) = \sum_{i=1}^{N} \alpha(i)\left[I(i,j) \cdot cos\left(\frac{\pi(2k+1)(i-1)}{2N}\right)\right] \tag{6}$$

where I is the $N \times N$ dimensional identity matrix, $\alpha(i) = \sqrt{1/N}$ when $i = 1$, and $\alpha(i) = \sqrt{2/N}$ when $i > 1$.

The coherence measure $\mu(\Phi, \Psi)$ defined in (3) is evaluated for the pair of the proposed measurement matrix ϕ and the IDCT sparse basis ψ. Matrix ϕ is normalized before the evaluation in accordance to Equation 2. The obtained coherence value is 3.46. For comparison purposes, a random matrix generated by Matlab *rand* function is also examined in the study. The coherence between the random matrix and the IDCT

sparse bases is 5.2. This shows that the proposed measurement matrix achieves about the same level of incoherence as random measurement matrices and hence confirms the suitability of the proposed measurement method in CS image applications.

The proposed measurement matrix does not satisfy RIP requirements. Note that RIP requirements are sufficient but not necessary conditions for recovering the original signal from CS measurements. For example, both RIP-2 and RIP-1, defined in Equation 1 with $p = 2$ and $p = 1$ respectively, guarantee signal recovery. A matrix that satisfies RIP-1 may not satisfy RIP-2, and vice versa. Further, RIP is a very strong condition guaranteeing the recovery of any signal, providing it is sufficiently sparse with respect to a properly chosen basis.

It has been shown that natural images generally have dominating low frequency components, and insignificant high frequency components. From [6] follows that the frequency spectrum of natural images along the frequency axis decays according to the equation:

$$A(f) = \frac{A_{DC}}{f^{\alpha}} \tag{7}$$

where A_{DC} and α represent the magnitude of the image DC component (proportional to the average pixel power) and decay rate along the frequency axis f respectively. Statistical data from a large number of images show that, on average, α is about 2.08, with an average standard deviation of 0.53 [6]. Thus, if a natural image is projected to the IDCT domain, the significant coefficients will be mainly distributed in the low frequency or low index region. Matlab simulations indicate that this is the key factor that enables the superb performance of the proposed CS measurement method.

To exemplify our finding, we use the proposed measurement matrix and a random measurement matrix, which satisfies RIP conditions, to conduct CS operations for two images. One is a common benchmark image Cameraman and the other is an artificially created image by alternately assigning one pixel to black, the next pixel to gray and the third pixel to white, as depicted in Fig. 2.

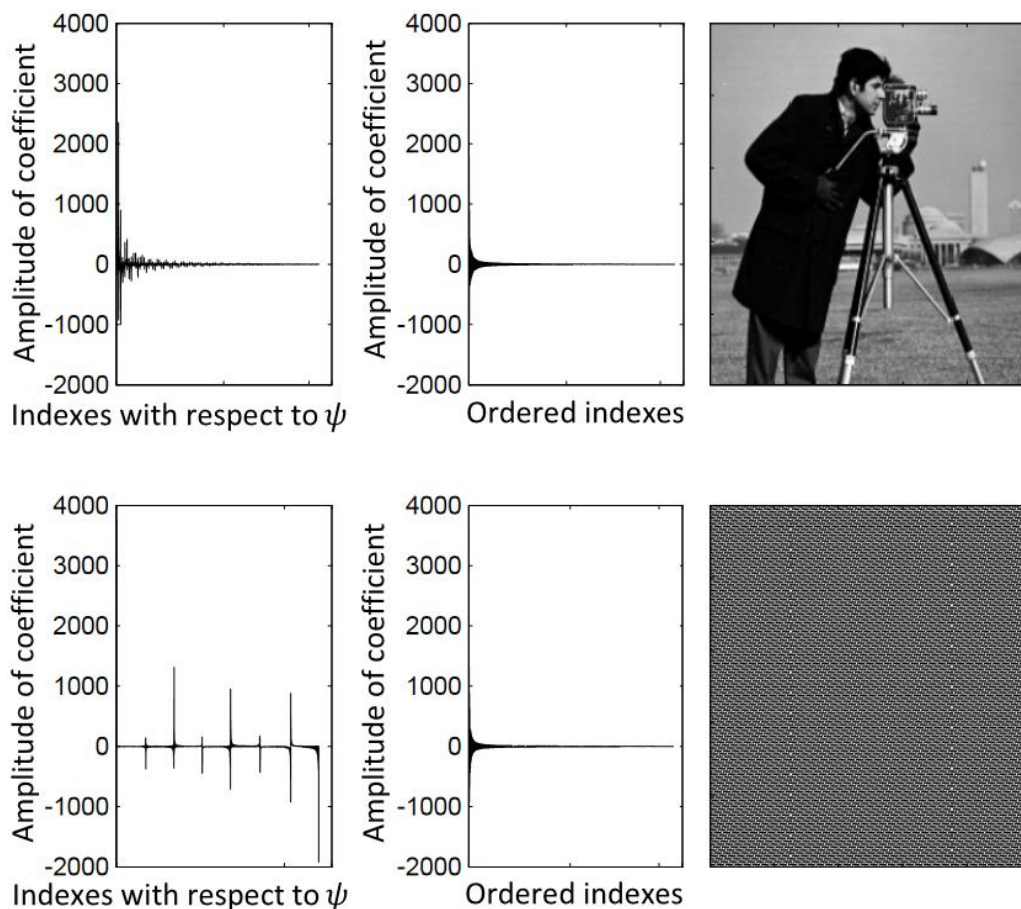Fig. 2. IDCT coefficients of Cameraman (top) and black-gray-white pattern (bottom)

Clearly, the artificial image does not exist in the real world since no natural images can exhibit such dramatic changes from one pixel to another, throughout the image. Both images are sparse with respect to the IDCT basis and their IDCT coefficients (coordinate vectors) are plotted in the left panel of fig. 2. For image Cameraman, its

significant coefficients concentrate in the low frequency region. However, the significant coefficients of the artificial image are scattered in a wide range. Despite this difference, the two images approximately have the same level of sparsity. This becomes evident after the coefficients are sorted in a descending order and plotted in the middle panel of the figure. In experiments using CS techniques to sample and recover image Cameraman, both the proposed and random measurement matrices lead to successful image reconstruction. Also, the proposed method results in a better image quality measured by peak signal to noise ratio (PSNR) [9]. This is mainly attributed to the fact that the CS measurements with using the proposed method better preserve local energy. With compression rate 4, the PSNR values with using the proposed and random measurement matrices are 32.7dB and 24.3dB, respectively. For the artificial image, the PSNR of the recovered image from the proposed CS measurements is only 12.3 dB. However, this image can still be recovered from the CS measurements using the random matrix. These observations support the earlier statements about the proposed and random measurement matrices. Nevertheless, the failure of recovering the artificial image from the proposed CS measurements should not be alarmed since such an image is unlikely to be seen in the real world.

Studies were also conducted via Matlab simulations to examine how widely the proposed CS measurement method can be applied to natural images. Without losing generality, sparse signals with a length of 2560 samples were used in the study. The sparsity of the signals is selected as 200. Thus, among the 2560 IDCT coefficients, 200 are significant and the remaining 2360 coefficients are negligible, which are at least 75 times smaller than the largest magnitude of the significant coefficients. A large set of

such sparse signals was generated by randomly varying the magnitudes and positions of the 200 significant coefficient terms. Then, the proposed and random matrices were used to generate CS measurements of these signals and later l_1 minimization techniques were used to recover the signals from their CS measurements.
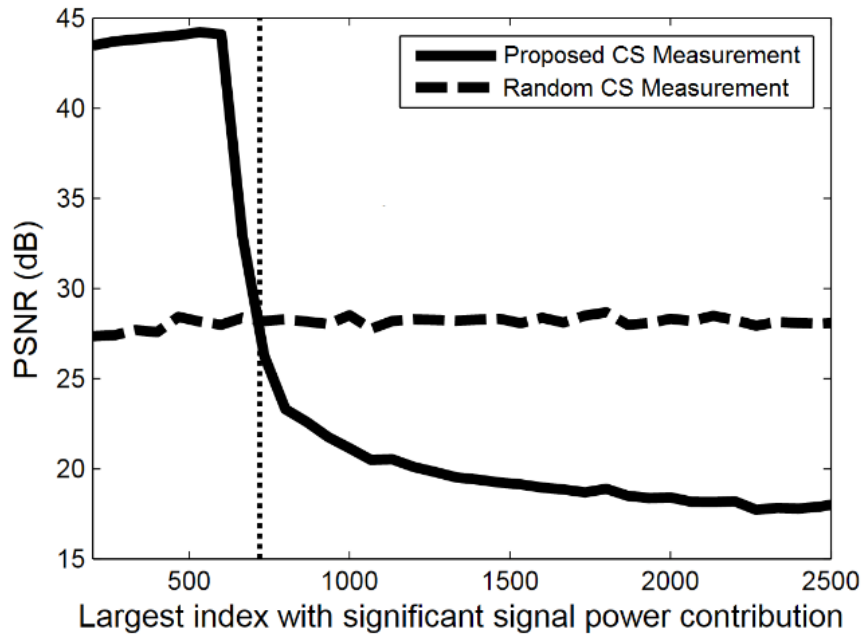
Fig. 3. Recovered signals from the proposed and random CS measurements with variable signal spectrum bandwidth

The PSNRs of the recovered signals using the proposed and random matrices are compared in Fig. 3. The horizontal axis indicates the highest index or frequency of the significant coefficients for a given signal. For example, if a data point in the figure has horizontal axis value of 500, then the significant coefficients of the corresponding signal are distributed in the region with indexes ranging from 1 to 500. The plot shows that, if the significant coefficients are distributed in the region with indexes smaller than 720 (the position marked by the dotted line in the figure), the proposed method outperforms the conventional random matrix based CS measurement method. Equation 7 indicates

that the maximum coefficient magnitude drops to about 1/75 of its DC value at the frequency corresponding to index 720, where α is approximately 0.67. This value is off from the average value of α by 2.66 times the standard deviation. This leads to the conclusion that the proposed method results in better image quality for about 99.6% of all natural images. If the significant coefficients are distributed in the region with index smaller than 600, which corresponds to 99.4% of natural images according to (7), the proposed CS measurement method results in significantly better image quality.

The proposed and the conventional random matrix-based CS measurement methods were applied to the two widely used benchmark images Lenna and Cameraman with different compression rates. The quality of the reconstructed images from the proposed and conventional CS measurements are shown in Fig. 4. The listed results clearly demonstrate the superiority of the proposed CS measurement method.
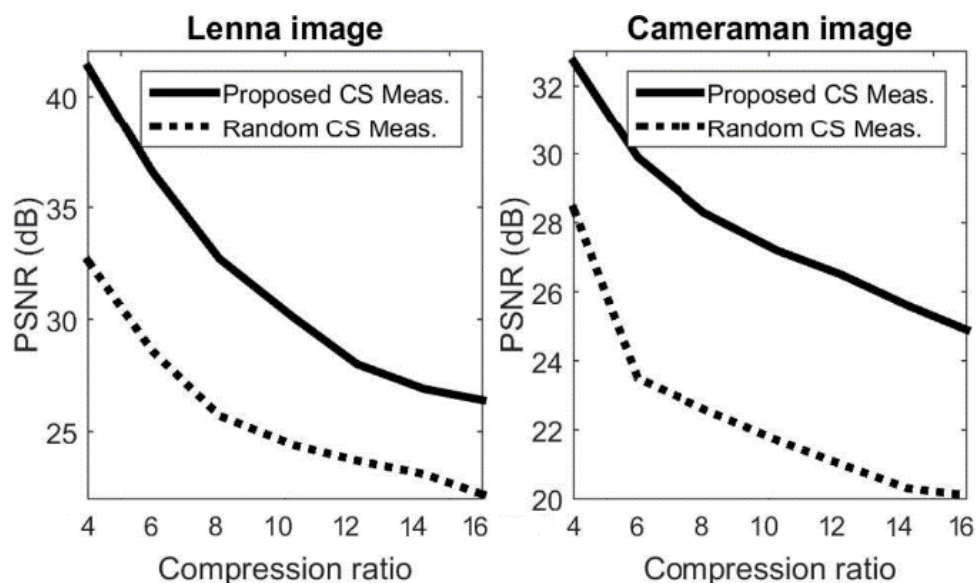

Fig. 4. Comparison of reconstructed image quality from the proposed and conventional CS measurements with variable compression rates

PERFORMANCE ESTIMATION

This section develops closed form expressions to evaluate the error between the original signals and the compressed or reconstructed data. Intuitive explanations are given in several instances, where a rigorous proof could not be found. This derivation therefore merely intends to collect ideas on how to quantify signal errors, rather than provide tight bounds for signal errors, and thus show validity of the proposed technique. Consider the previously introduced notations:

- Original discrete signal x of length N

- Compressed signal y of length M

- Measurement matrix Φ of dimension M, N

- Compression rate R

- Sparse representation bases Ψ of dimension N, N

- Coordinate vector $[s]_\Psi$ of x w.r.t. Ψ

As discussed in the introduction and background sections, signals under consideration must satisfy the following criteria:

a) Sparsity: When projecting signal x onto representation bases Ψ, only at most $N^*_{[s]}$ out of N coefficients are significant in coordinate vector $[s]_\Psi$. Define a coefficient s_i to be significant if its magnitude is not less than P-% of that of the largest coefficients.

b) Dominant low- frequency components: The bulk of the signal power is carried by low frequency components, i.e., coefficients corresponding to low frequency bases vectors are large, while high frequency components

have, in general, small coefficients. In particular, (7) is altered to obtain the more practical model:

$$|s_j| \leq C_N + \frac{C_{DC}}{j^\alpha} \qquad 1 \leq j \leq N \tag{8}$$

where C_N and C_{DC} are the magnitude of high frequency (noise) components and the magnitude of the DC- or dominant low frequency component respectively. α is the decay rate along the frequency axes, obtained from statistical data of natural images.

The entries in Ψ originate from the inverse discrete cosine transform. A simplified and slightly modified version of the expression in (6) is given by:

$$\Psi(i,j) = C_j \cdot \cos\left(\frac{\pi(j-1)(i-1)}{N}\right) \tag{9}$$

with $C_1 = \sqrt{1/N}$ and $C_j = \sqrt{2/N}$ for $j = 2, \dots, N$. Note that these constants lead to unified signal power of all j columns of Ψ. With the help of $x = \Psi \cdot [s]_\Psi$, the signal can be represented as:

$$x(i) = \sum_{j=1}^{N} s_j \cdot \Psi(i,j) = \sum_{j=1}^{N} s_j \cdot C_j \cdot \cos\left(\frac{\pi(j-1)(i-1)}{N}\right) \tag{10}$$

with unique coefficients $s_1, s_2, \dots, s_N$ for any given signal $x \in \Re^n$.

To compute bounds for the minimum signal quality, it is necessary to quantify how much the signal can deviate from the measurement value, which is the average of the samples in the measurement support. Thus, this measure depends on the rate of change of x along index i. The average, root mean square (RMS), and maximum slope of the signal are three potential candidates to quantify the rate of change of x. By definition of PSNR, the squared difference between the original and reconstructed

signals is accumulated. Thus absolute differences are weighted with a power of two. The same is true for the definition of the root mean square value of a continuous function, which also is a measure of the squared magnitudes. This suggests that the RMS slope should be the main component when quantifying signal rate of change. The first step is to compute these slopes, which for simplification purposes, is partially carried out in the continuous domain.

A. Upper bound for maximum slope of x along i:

From (10) the maximum rate of change of x along i can be approximated in the continuous domain by:

$$\max_i \left| \frac{dx(i)}{di} \right| \approx \max_i \left| \frac{d}{di} \left(\int_{j=1}^{N} s_j \cdot C_j \cdot \cos \left(\frac{\pi(j-1)(i-1)}{N} \right) dj \right) \right|. \tag{11}$$

Unfortunately, the above formula has no explicit solution. In the discrete domain $\frac{\Delta x(i)}{\Delta i}$ follows from (10) as:

$$\frac{\Delta x(i)}{\Delta i} = -\sum_{j=1}^{N} s_j \cdot C_j \cdot \left(\frac{\pi(j-1)}{N} \right) \cdot \sin \left(\frac{\pi(j-1)(i-1)}{N} \right). \tag{12}$$

Similarly, it follows from (10) that:

$$\max_i \left| \frac{\Delta x(i)}{\Delta i} \right| = \max_i |\Delta x(i)| \approx \max_{1 \leq k \leq N-1} |x(k) - x(k+1)|$$

$$= \max_{1 \leq k \leq N-1} \left| \sum_{j=1}^{N} s_j \cdot C_j \cdot \left[\cos \left(\frac{\pi(j-1)(k-1)}{N} \right) - \cos \left(\frac{\pi(j-1)k}{N} \right) \right] \right| \tag{13}$$

with $\Delta i = 1$. Coefficients s_j are, in general, unknown, so that it is difficult to find a tight upper bound of the distance among two consecutive entries of x for all possible signals

satisfying the above properties. The slope of the cosine is maximally one, and the argument of the cosine functions differs by a factor $\left(\frac{\pi(j-1)}{N}\right)$. Thus it follows that:

$$\max_i |\Delta\, x(i)| \leq \sum_{j=1}^{N} s_j \cdot C_j \cdot \left(\frac{\pi(j-1)}{N}\right) \qquad (14)$$

which becomes immediately clear also from (12). By definition $C_1 = \sqrt{1/N}$ and $C_j = \sqrt{2/N}$ for $j = 2, \dots, N$. Since this estimation is to compute the rate of change of signal x, the constant term, whose magnitude is C_1, has no impact. Note that this is congruent with term $(j-1)$ in the sum, which vanishes when $j = 1$. Going back to the continuous domain, $\max_i |\Delta\, x(i)|$ can be determined as follows:

$$\begin{aligned}
\max_i |\Delta\, x(i)| &\leq \sum_{j=1}^{N} s_j \cdot C_j \cdot \left(\frac{\pi(j-1)}{N}\right) \leq \sum_{j=1}^{N} \left(C_N + \frac{C_{DC}}{j^\alpha}\right) \cdot C_j \cdot \left(\frac{\pi(j-1)}{N}\right) \\
&\approx \int_{j=1}^{N} (C_N + C_{DC} \cdot j^{-\alpha}) \cdot C_j \cdot \left(\frac{\pi(j-1)}{N}\right) dj \\
&= \frac{C_N \cdot C_j \cdot \pi}{N} \int_{j=1}^{N} (j-1)dj + \frac{C_{DC} \cdot C_j \cdot \pi}{N} \int_{j=1}^{N} j^{-\alpha}(j-1)dj \\
&= \frac{C_N \cdot C_j \cdot \pi}{N} \left[\frac{j^2}{2} - j\right]_{j=1}^{N} + \frac{C_{DC} \cdot C_j \cdot \pi}{N} \left[\frac{j^{2-\alpha}}{2-\alpha} - \frac{j^{1-\alpha}}{1-\alpha}\right]_{j=1}^{N} \\
&= \frac{C_N \cdot C_j \cdot \pi}{N} \left[\frac{j^2}{2} - j\right]_{j=1}^{N} + \frac{C_{DC} \cdot C_j \cdot \pi}{N} \left[\frac{j^{1-\alpha}(-j \cdot \alpha + \alpha + j - 2)}{(\alpha-2)(\alpha-1)}\right]_{j=1}^{N} \\
&= \frac{C_N \cdot C_j \cdot \pi}{N} \left(\frac{N^2}{2} - N + \frac{1}{2}\right) + \frac{C_{DC} \cdot C_j \cdot \pi}{N} \left(\frac{N^{1-\alpha}(-N \cdot \alpha + \alpha + N - 2) + 1}{(\alpha-2)(\alpha-1)}\right).
\end{aligned}$$

$$(15)$$

Note that:

$$\lim_{\alpha \to 1} \frac{N^{1-\alpha}(-N \cdot \alpha + \alpha + N - 2) + 1}{(\alpha - 2)(\alpha - 1)} = \frac{"0"}{"0"}$$

$$= \lim_{\alpha \to 1} \frac{\frac{d}{d\alpha}(N^{1-\alpha}(-N \cdot \alpha + \alpha + N - 2) + 1)}{\frac{d}{d\alpha}(\alpha - 2)(\alpha - 1)} \qquad (16)$$

$$\lim_{\alpha \to 1} \frac{-N^{1-\alpha}\ln(N)(-N \cdot \alpha + \alpha + N - 2) + N^{1-\alpha}(-N + 1)}{2\alpha - 3} = N - 1 - \ln(N) \geq 0.$$

Similarly:

$$\lim_{\alpha \to 2} \frac{N^{1-\alpha}(-N \cdot \alpha + \alpha + N - 2) + 1}{(\alpha - 2)(\alpha - 1)} = \frac{"0"}{"0"}$$

$$= \lim_{\alpha \to 2} \frac{\frac{d}{d\alpha}(N^{1-\alpha}(-N \cdot \alpha + \alpha + N - 2) + 1)}{\frac{d}{d\alpha}(\alpha - 2)(\alpha - 1)} \qquad (17)$$

$$\lim_{\alpha \to 2} \frac{-N^{1-\alpha} \cdot \ln(N)(-N \cdot \alpha + \alpha + N - 2) + N^{1-\alpha}(-N + 1)}{2\alpha - 3} = \ln(N) + N^{-1} - 1 \geq 0$$

for all $N > 0$. Thus above result is well defined for any $\alpha > 0$, and $\max_i |\Delta x(i)|$ can be

bounded above by:

$$(18)$$

$$\max_i |\Delta x(i)| \leq \frac{C_N \cdot C_j \cdot \pi}{N}\left(\frac{N^2}{2} - N + \frac{1}{2}\right) + \frac{C_{DC} \cdot C_j \cdot \pi}{N}\left(\frac{N^{1-\alpha}(-N \cdot \alpha + \alpha + N - 2) + 1}{(\alpha - 2)(\alpha - 1)}\right).$$

A. Upper bound for Average absolute slope of **x** along **i**:

The estimation of the average slope requires the evaluation of:

$$\operatorname*{avg}_i\left(\frac{dx(i)}{di}\right) = \frac{1}{N}\int_{i=1}^{N} \left|\frac{d}{di}\left(\int_{j=1}^{N} s_j \cdot C_j \cdot \cos\left(\frac{\pi(j-1)(i-1)}{N}\right) dj\right)\right| di \qquad (19)$$

for which no closed form solution exists. In addition, since the form factor for general

signal x is unknown, no relation is possible between the RMS and average value of the

slope of x. It is however in general true that the average value is smaller than or equal

to the RMS value, and the closed form solution for the upper bound of the RMS slope is given below. In addition, the maximum slope being much larger than the RMS slope indicates that the average slope is much smaller than the RMS slope. However, it is difficult to quantify in general how large this difference is.

B. Upper bound for Root Mean Square slope of $\mathbf{x}$ along $\mathbf{i}$:

The Root Mean Square (RMS) slope of x along i can be defined with the help of (12) and the definition of RMS as:

$$\underset{i}{rms}(\Delta\,x(i)) = \sqrt{\frac{1}{N}\sum_{i=1}^{N}(\Delta\,x(i))^2}$$

$$= \sqrt{\frac{1}{N}\sum_{i=1}^{N}\left(-\sum_{j=1}^{N}s_j\cdot C_j\cdot\left(\frac{\pi(j-1)}{N}\right)\sin\left(\frac{\pi(j-1)(i-1)}{N}\right)\right)^2}$$

(20)

The expression under the quadrat can be divided into two parts. First, the product of every term with itself, and second, all permutations of terms with different arguments in the sinusoids:

$$\left(\sum_{j=1}^{N}s_j\cdot C_j\cdot\left(\frac{\pi(j-1)}{N}\right)\sin\left(\frac{\pi(j-1)(i-1)}{N}\right)\right)^2$$

$$= \sum_{j=1}^{N}\left(s_j\cdot C_j\cdot\left(\frac{\pi(j-1)}{N}\right)\sin\left(\frac{\pi(j-1)(i-1)}{N}\right)\right)^2$$

(21)

(22)

$$+ \sum_{\substack{j=1,2,\dots,N\\k=1,2,\dots,N\\j\neq k}}s_j s_k C_j C_k\frac{\pi^2}{N^2}(j-1)(k-1)\sin\left(\frac{\pi(j-1)(i-1)}{N}\right)\sin\left(\frac{\pi(k-1)(i-1)}{N}\right).$$

Note that:

$$\int_0^{n\cdot\pi} \sin(k\cdot x)\sin(j\cdot x)\,dx$$

$$= \left[\frac{-\dfrac{\cos(k\cdot x)\sin(j\cdot x)}{k} + \dfrac{j\cdot\sin(k\cdot x)\cos(j\cdot x)}{k^2}}{1-\left(\dfrac{j}{k}\right)^2}\right]_{x=0}^{i\cdot\pi} = 0 \tag{23}$$

for all integers k, j and i, if $k \neq j$. That is, the integral over the product of two sinusoids with different integer arguments over a multiple of half-periods is zero. Computing the average of expression (22) over all i as necessary to obtain (20) yields:

$$\tag{24}$$

$$\frac{1}{N}\sum_{i=1}^{N}\sum_{\substack{j=1,2,\dots,N\\k=1,2,\dots,N\\j\neq k}} s_j s_k C_j C_k \frac{\pi^2}{N^2}(j-1)(k-1)\sin\left(\frac{\pi(j-1)(i-1)}{N}\right)\sin\left(\frac{\pi(k-1)(i-1)}{N}\right).$$

The order of addition can be interchanged, so that (24) can be simplified to:

$$\tag{25}$$

$$\sum_{\substack{j=1,2,\dots,N\\k=1,2,\dots,N\\j\neq k}} s_j s_k C_j C_k \frac{\pi^2}{N^3}(j-1)(k-1)\sum_{i=1}^{N}\sin\left(\frac{\pi(j-1)(i-1)}{N}\right)\sin\left(\frac{\pi(k-1)(i-1)}{N}\right).$$

The internal sum in (25) is the discrete version of integral (23). The sum is performed over all i from 1 to N, where the arguments of the sine functions span the intervals 0 to approximately $\pi(j-1)$ and $\pi(k-1)$ respectively, assuming N is not very small. By the result in (23) it is therefore reasonable to assume that expression (25) is approximately zero.

Now, (20) simplifies to:

$$rms_i(\Delta\,x(i)) \approx \sqrt{\frac{1}{N}\sum_{i=1}^{N}\sum_{j=1}^{N}\left(s_j \cdot C_j \cdot \left(\frac{\pi(j-1)}{N}\right)\sin\left(\frac{\pi(j-1)(i-1)}{N}\right)\right)^2} \qquad (26)$$

and can be rearranged to the even simpler form:

$$rms_i(\Delta\,x(i)) \approx \sqrt{\sum_{j=1}^{N}\left(s_j \cdot C_j \cdot \left(\frac{\pi(j-1)}{N}\right)\right)^2 \frac{1}{N}\sum_{i=1}^{N}\left(\sin\left(\frac{\pi(j-1)(i-1)}{N}\right)\right)^2}. \qquad (27)$$

But $\frac{1}{N}\sum_{i=1}^{N}\left(\sin\left(\frac{\pi(j-1)(i-1)}{N}\right)\right)^2$ is the squared and discrete version of the general equation

for computing the RMS value of any continuous function $y(t)$ in the interval $[a,b]$ given

by:

$$RMS_{y(t)}^2 = \frac{1}{b-a}\int_{a}^{b}\left(y(t)\right)^2 dt. \qquad (28)$$

It is well known that the RMS value of the sinusoidal waveform over an interval, which is

a multiple of π, is equal to $1/\sqrt{2}$. It follows that:

$$\frac{1}{N}\sum_{i=1}^{N}\left(\sin\left(\frac{\pi(j-1)(i-1)}{N}\right)\right)^2 \approx \frac{1}{2} \qquad (29)$$

Thus (27) becomes:

$$rms_i(\Delta\,x(i)) \approx \sqrt{\frac{1}{2}\sum_{j=1}^{N}\left(s_j \cdot C_j \cdot \left(\frac{\pi(j-1)}{N}\right)\right)^2}$$

$$\approx \sqrt{\frac{1}{2}\int_{j=1}^{N}\left(s_j \cdot C_j \cdot \left(\frac{\pi(j-1)}{N}\right)\right)^2 dj} \qquad (30)$$

$$\leq \sqrt{\frac{1}{2}\int_{j=1}^{N}\left((C_N + C_{DC}\cdot j^{-\alpha})\cdot C_j \cdot \left(\frac{\pi(j-1)}{N}\right)\right)^2 dj}.$$

As discussed earlier, the constant term in the sum has no impact, so that $C_j = \sqrt{2/N}$ can be chosen for all $j = 1, \ldots, N$. Thus:

$$\left(\underset{i}{rms}(\Delta x(i))\right)^2 \leq \frac{1}{2}\left(\frac{C_N \cdot C_j \cdot \pi}{N}\right)^2 \int_{j=1}^{N}(j-1)^2 dj$$

$$+ C_N \cdot C_{DC}\cdot\left(\frac{C_j \cdot \pi}{N}\right)^2 \int_{j=1}^{N}j^{-\alpha}(j-1)^2 dj$$

$$+\frac{1}{2}\left(\frac{C_{DC} \cdot C_j \cdot \pi}{N}\right)^2 \int_{j=1}^{N}j^{-2\cdot\alpha}(j-1)^2 dj$$

$$= \frac{1}{2}\left(\frac{C_N \cdot C_j \cdot \pi}{N}\right)^2 \left[\frac{j^3}{3} - j^2 + j\right]_{j=1}^{N} \tag{31}$$

$$-C_N \cdot C_{DC}\cdot\left(\frac{C_j \cdot \pi}{N}\right)^2 \left[\frac{j^{1-\alpha}\left(\alpha^2(j-1)^2 + \alpha(-3j^2 + 8j - 5) + 2(j^2 - 3j + 3)\right)}{(\alpha-3)(\alpha-2)(\alpha-1)}\right]_{j=1}^{N}$$

$$-\frac{1}{2}\left(\frac{C_{DC} \cdot C_j \cdot \pi}{N}\right)^2 \left[\frac{j^{1-2\cdot\alpha}\left(2\alpha^2(j-1)^2 + \alpha(-3j^2 + 8j - 5) + j^2 - 3j + 3\right)}{(2\alpha-1)(2\alpha-3)(\alpha-1)}\right]_{j=1}^{N}$$

$$= \frac{1}{2}\left(\frac{C_N \cdot C_j \cdot \pi}{N}\right)^2 \left(\frac{N^3}{3} - N^2 + N - \frac{1}{3}\right)$$

$$+C_N \cdot C_{DC}\cdot\left(\frac{C_j \cdot \pi}{N}\right)^2 \left(\frac{2 - N^{1-\alpha}\left(\alpha^2(N-1)^2 + \alpha(-3N^2 + 8N - 5) + 2(N^2 - 3N + 3)\right)}{(\alpha-3)(\alpha-2)(\alpha-1)}\right)$$

$$+\frac{1}{2}\left(\frac{C_{DC} \cdot C_j \cdot \pi}{N}\right)^2 \left(\frac{1 - N^{1-2\cdot\alpha}\left(2\alpha^2(N-1)^2 + \alpha(-3N^2 + 8N - 5) + N^2 - 3N + 3\right)}{(2\alpha-1)(2\alpha-3)(\alpha-1)}\right).$$

Using L'Hospital's rule it can be shown that, (31) is well defined for all α grater zero. The desired result is then given by:

$$rms_i(\Delta x(i)) \le \left[\frac{1}{2}\left(\frac{C_N \cdot C_j \cdot \pi}{N}\right)^2 \left(\frac{N^3}{3} - N^2 + N - \frac{1}{3}\right)\right.$$

$$+ C_N \cdot C_{DC} \cdot \left(\frac{C_j \cdot \pi}{N}\right)^2 \left(\frac{2 - N^{1-\alpha}\left(\alpha^2(N-1)^2 + \alpha(-3N^2 + 8N - 5) + 2(N^2 - 3N + 3)\right)}{(\alpha-3)(\alpha-2)(\alpha-1)}\right)$$

$$\left. + \frac{1}{2}\left(\frac{C_{DC} \cdot C_j \cdot \pi}{N}\right)^2 \left(\frac{1 - N^{1-2\cdot\alpha}(2\alpha^2(N-1)^2 + \alpha(-3N^2 + 8N - 5) + N^2 - 3N + 3)}{(2\alpha-1)(2\alpha-3)(\alpha-1)}\right)\right]^{\frac{1}{2}}.$$

B. Sparsity consideration:

In the estimation of (18) and (32), coefficients $|s_j|$ are expressed as $C_N + \frac{C_{DC}}{j^\alpha}$. In reality, function $C_N + \frac{C_{DC}}{j^\alpha}$ bounds coefficients $|s_j|$, but typically only a (small) subset of all coefficients has a magnitude significantly large to have a notable contribution to the harmonic signal representation. Defining a relative magnitude of at least P-% as significant, the maximum number of significant coefficients $N_{[s]}^{\max}$ is given by:

$$\frac{1}{\left(N_{[s]}^{\max}\right)^\alpha} = \frac{P(\%)}{100\%} \rightarrow N_{[s]}^{\max} \approx \left(\frac{100}{P(\%)}\right)^{\frac{1}{\alpha}} \tag{33}$$

with the limitation that $N_{[s]}^{\max} \le N$. Assuming the signal has a sparsity of $N_{[s]}^*$, $N_{[s]}^{\max} - N_{[s]}^*$ coefficients are insignificant under the envelope described by (8). The distribution of the significant coefficients is, in general, unknown. While magnitudes drop proportionally to $\frac{1}{j^\alpha}$, the rate of change of their corresponding sinusoid increases according to $(j - 1) \approx j$. Since $\frac{j}{j^\alpha} = j^{1-\alpha}$, it depends on α which coefficients carry the largest weight of the signal. If $\alpha \ll 1$, coefficients with indexes close to $N_{[s]}^{\max}$ are dominant. If $\alpha \gg 1$, coefficients with small indexes are dominant. Assuming the dominant coefficients are approximately

equally distributed in the window $1\ to\ N_{[s]}^{\max}$, and assuming $|1 - \alpha|$ is small, selecting the

subset of $N_{[s]}^*$ dominant coefficients is approximately equivalent to assuming all

coefficients are significant, scaled by the ratio $N_{[s]}^*/N_{[s]}^{\max}$. This is because, in that

particular case, all coefficients carry approximately the same weight. (18) and (32) are

then modified respectively as follows:

$$\max_i |\Delta\, x(i)| \leq \frac{C_N \cdot C_j \cdot \pi}{N}\left(\frac{N^2}{2} - N + \frac{1}{2}\right)$$

$$+\frac{N_{[s]}^* \cdot C_{DC} \cdot C_j \cdot \pi}{N_{[s]}^{\max} \cdot N}\left(\frac{N^{1-\alpha}(-N \cdot \alpha + \alpha + N - 2) + 1}{(\alpha - 2)(\alpha - 1)}\right) \tag{34}$$

$$rms_i(\Delta\, x(i)) \leq \left[\frac{1}{2}\left(\frac{C_N \cdot C_j \cdot \pi}{N}\right)^2\left(\frac{N^3}{3} - N^2 + N - \frac{1}{3}\right) + C_N \cdot C_{DC} \cdot \frac{N_{[s]}^*}{N_{[s]}^{\max}}\right.$$

$$\left(\frac{C_j \cdot \pi}{N}\right)^2\left(\frac{2 - N^{1-\alpha}\left(\alpha^2(N-1)^2 + \alpha(-3N^2 + 8N - 5) + 2(N^2 - 3N + 3)\right)}{(\alpha - 3)(\alpha - 2)(\alpha - 1)}\right) \tag{35}$$

$$\left.+\frac{1}{2}\left(\frac{N_{[s]}^* \cdot C_{DC} \cdot C_j \cdot \pi}{N_{[s]}^{\max} \cdot N}\right)^2\left(\frac{1 - N^{1-2\cdot\alpha}(2\alpha^2(N-1)^2 + \alpha(-3N^2 + 8N - 5) + N^2 - 3N + 3)}{(2\alpha - 1)(2\alpha - 3)(\alpha - 1)}\right)\right]^{\frac{1}{2}}.$$

C. Minimum signal quality of compressed signal

The measurement matrices used in this discussion sum a small number of

neighboring samples, without overlap among neighboring measurement supports. The

k^{th} sum $y(k)$ can be conveniently described as:

$$y(k) = \sum_{i=1+R(k-1)}^{R\cdot k} x(i) \tag{36}$$

for $k = 1, \dots, M$. Employing these matrices, the signal power of the small groups of

neighboring samples is precisely known. It is easily possible to even it out among

neighboring samples of the same measurement subgroup, ie., to compute the average

power of the samples included in a particular support. This yields a minimum signal

quality which can always be achieved. The goal in this subsection is to quantify the error

of the compressed signal with respect to the original signal, and to find an upper bound

of the same.

The question is, what compressed- original signal combination results in the

largest accumulated squared error, with the constraint that the averaged actual signal

trajectory equals the measurement value. Figures 5 and 6 show two extreme cases with

zero and large variation among neighboring measurement supports. In both cases, the

solid line represents the averaged sample values, the dashed trajectory a possible

actual signal path, with maximum accumulated error with respect to the measurement

value. As discussed earlier, the slope of the dashed line is assumed to be limited by the

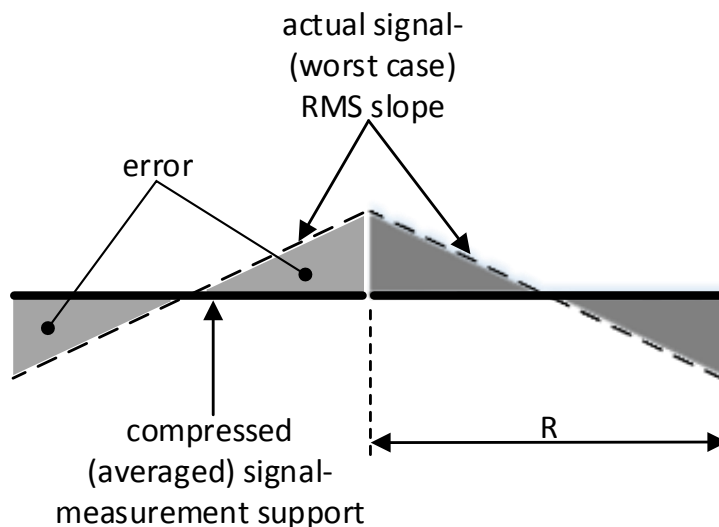RMS slope computed in (35).

Fig. 5. Maximum difference among compressed and original signals
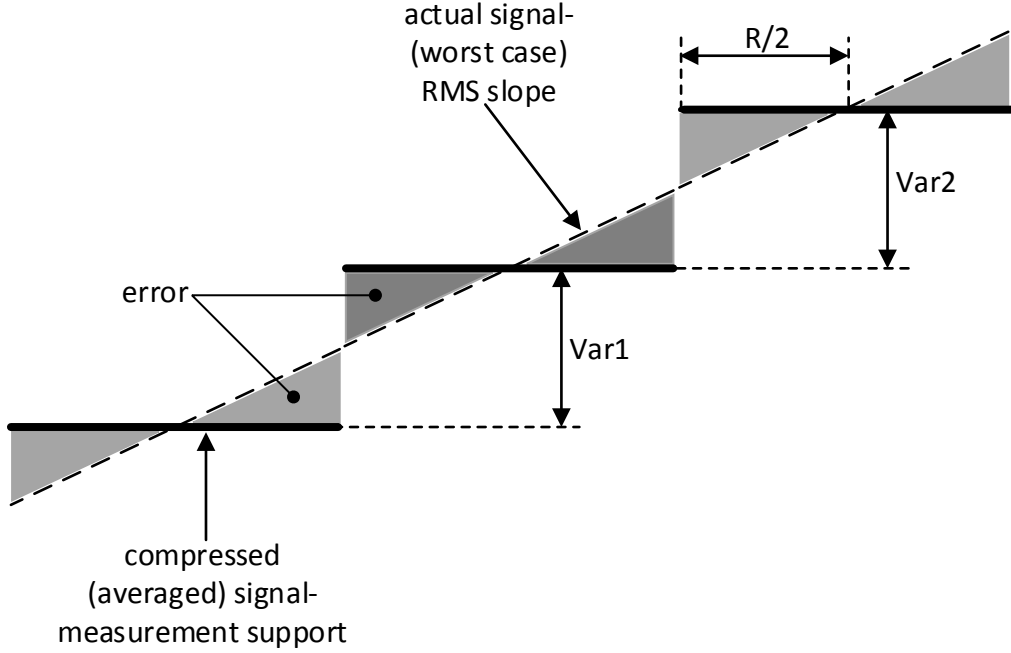with constant measurement values

Fig. 6. Maximum difference among compressed and original signals
with monotonic and largely variant measurement values

From fig. 5 and 6 follows that the squared error of one measurement of the compressed

and averaged signal $x'(i)$ containing R samples is bounded above by:

$$\sum_{i=1+R(k-1)}^{R \cdot k} \left(x(i) - x'(i)\right)^2 \leq 2 \int_0^{\frac{R}{2}} \left(\underset{i}{rms}(\vartriangle x(i)) \cdot x\right)^2 dx$$

$$= 2 \left(\underset{i}{rms}(\vartriangle x(i))\right)^2 \frac{R^3}{24} = \frac{R^3}{12} \left(\underset{i}{rms}(\vartriangle x(i))\right)^2$$

(37)

assuming the worst case when the actual signal sweeps with a slope of $\underset{i}{rms}(\vartriangle x(i))$

throughout the measurement support. The accumulated squared error over all

measurements is then bounded above by:

$$\sum_{i=1}^{N}\left(x(i) - x'(i)\right)^2 = \frac{N}{R} \cdot \sum_{i=1+R(k-1)}^{R \cdot k} \left(x(i) - x'(i)\right)^2 = \frac{N}{R}\frac{R^3}{12} \left(\underset{i}{rms}(\vartriangle x(i))\right)^2$$

(38)

$$= \frac{N \cdot R^2}{12} \left(\underset{i}{rms}(\Delta x(i)) \right)^2.$$

The mean square error (average squared error) follows as:

$$MSE_{MAX} = \frac{R^2}{12} \left(\underset{i}{rms}(\Delta x(i)) \right)^2 \tag{39}$$

and the PSNR is defined as:

$$PSNR(dB) = -10 \cdot \log_{10} \left(\frac{MSE}{S^2} \right) \tag{40}$$

where S is the maximum value a sample (or pixel value in image processing) can take on. Finally, with the help of (36), (39) and (40), the minimum PSNR can be determined using:

$$\tag{41}$$

$$SNR(dB) = -10 \cdot \log_{10} \left\{ \frac{R^2}{12 \cdot S^2} \left[\frac{1}{2} \left(\frac{C_N \cdot C_j \cdot \pi}{N} \right)^2 \left(\frac{N^3}{3} - N^2 + N - \frac{1}{3} \right) + C_N \cdot C_{DC} \cdot \frac{N^*_{[s]}}{N^{\max}_{[s]}} \right. \right.$$

$$\left(\frac{C_j \cdot \pi}{N} \right)^2 \left(\frac{2 - N^{1-\alpha} \left(\alpha^2 (N-1)^2 + \alpha(-3N^2 + 8N - 5) + 2(N^2 - 3N + 3) \right)}{(\alpha - 3)(\alpha - 2)(\alpha - 1)} \right)$$

$$\left. \left. + \frac{1}{2} \left(\frac{N^*_{[s]} \cdot C_{DC} \cdot C_j \cdot \pi}{N^{\max}_{[s]} \cdot N} \right)^2 \frac{1 - N^{1-2\cdot\alpha} (2\alpha^2 (N-1)^2 + \alpha(-3N^2 + 8N - 5) + N^2 - 3N + 3)}{(2\alpha - 1)(2\alpha - 3)(\alpha - 1)} \right] \right\}.$$

Note that this limit is a theoretical minimum giving a theoretical lowest possible PSNR for all signals of length N satisfying the sparsity and low frequency condition.

To find a tighter lower bound for the minimum PSNR, and to further categorize the types of signals, introduce the following two additional parameters, further adding information about the signal:

c) Define by Var the average absolute variation between two measurements. Note that the knowledge of coefficient vector $[s]_\Psi$ gives an upper bound for

Var, but no lower bound. $Var = 0$ is possible for arbitrary coefficients s_j.

The maximum possible average variation is given by the average slope

along x times R. Thus Var calculated from the measurements has to be

smaller than $avg_i(\Delta x(i)) \cdot R$. Naturally define:

$$0 \leq Var = \frac{1}{M-1} \sum_{i=1}^{M-1} |y(i) - y(i+1)| \leq avg_i(\Delta x(i)) \cdot R \tag{42}$$

d) Another factor influencing the recovered signal-s quality is the

monotonicity of the measurements. Are the measurements mostly

continuously in- or decreasing or do they in- and decrease randomly? As

discussed later, the less monotonic a signal, the better the quality of the

reconstructed image. Thus define by β the monotonicity of the

measurements. Let $\beta = 1$ if the number of measurements larger than their

predecessor is approximately equal to the number of measurements

smaller than their predecessor (as in Fig. 7). Let $\beta = 0$ if all measurements

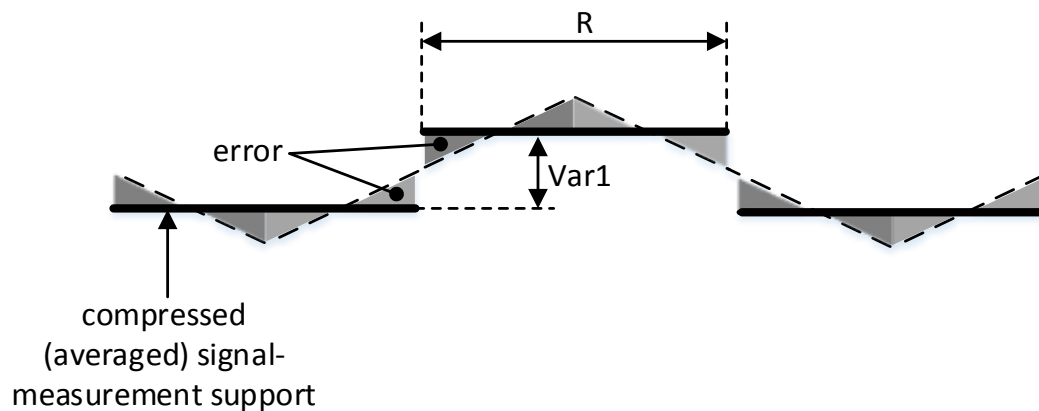are larger/smaller than their predecessor (as in Fig. 6).

Fig. 7. Maximum difference among compressed and original signals
with non-monotonic and largely variant measurement values

If $\beta = 1$ and $Var = \underset{i}{avg}(\Delta\, x(i)) \cdot R$ as shown in Fig. 7, the maximum error of the compressed signal reduces to:

$$\sum_{i=1+R(k-1)}^{R \cdot k} \left(x(i) - x'(i)\right)^2 \leq 4 \int_0^{\frac{R}{4}} \left(\underset{i}{rms}(\Delta\, x(i)) \cdot x\right)^2 dx$$

$$= 4 \left(\underset{i}{rms}(\Delta\, x(i))\right)^2 \frac{R^3}{192} = \frac{R^3}{48} \left(\underset{i}{rms}(\Delta\, x(i))\right)^2.$$

(43)

The mean square error then follows as:

$$MSE_{MIN} = \frac{R^2}{48} \left(\underset{i}{rms}(\Delta\, x(i))\right)^2$$

(44)

which is four times smaller than MSE_{MAX}. Now, if Var and/or β is zero, the mean square error is bounded by the result in (39). In the other extreme when Var and β is one, (44) gives a lower bound for the accumulated error. Table 1 summarizes the four extreme cases as a function of Var and β.

Table. 1. Mean Square Error as a function of Variation and
Monotonicity of the compressed signal

	$\beta = 0$	$\beta = 1$
$Var = 0$	$MSE = MSE_{MAX}$	$(MSE = MSE_{MAX})$
$Var = R \cdot \underset{i}{avg}(\Delta\, x(i))$	$MSE = MSE_{MAX}$	$MSE = MSE_{MIN}$

Thus incorporating a linear shift determined by Var and β between the minimum and maximum variation and monotonicity cases in MSE yields:

$$MSE = \frac{R^2}{12}\left(1 - \frac{3}{4}\frac{Var \cdot \beta}{R \cdot \underset{i}{avg}(\Delta\, x(i))}\right)\left(\underset{i}{rms}(\Delta\, x(i))\right)^2. \tag{45}$$

Thus the minimum guaranteed PSNR as a function of signal length N, signal strength S, compression rate R, variation Var, monotonicity β, frequency decay rate α and magnitudes C_N, C_{DC} can be determined using:

(46)

$$SNR(dB) = -10 \cdot \log_{10}\left\{\frac{R^2}{12 \cdot S^2}\left(1 - \frac{3}{4}\frac{Var \cdot \beta}{R \cdot \underset{i}{avg}(\Delta\, x(i))}\right)\right.$$

$$\left[\frac{1}{2}\left(\frac{C_N \cdot C_j \cdot \pi}{N}\right)^2\left(\frac{N^3}{3} - N^2 + N - \frac{1}{3}\right) + C_N \cdot C_{DC} \cdot \frac{N_{[s]}^*}{N_{[s]}^{\max}}\right.$$

$$\left(\frac{C_j \cdot \pi}{N}\right)^2\left(\frac{2 - N^{1-\alpha}\left(\alpha^2(N-1)^2 + \alpha(-3N^2 + 8N - 5) + 2(N^2 - 3N + 3)\right)}{(\alpha-3)(\alpha-2)(\alpha-1)}\right)$$

$$\left.\left.+ \frac{1}{2}\left(\frac{N_{[s]}^* \cdot C_{DC} \cdot C_j \cdot \pi}{N_{[s]}^{\max} \cdot N}\right)^2\frac{1 - N^{1-2\cdot\alpha}(2\alpha^2(N-1)^2 + \alpha(-3N^2 + 8N - 5) + N^2 - 3N + 3)}{(2\alpha-1)(2\alpha-3)(\alpha-1)}\right]\right\}$$

D. Minimum signal quality of reconstructed signal

If the entire image frame is homogeneous, i.e., all measurements result in approximately the same value, the compressed signal does not differ from the reconstructed signal, since a homogeneous solution is the sparsest solution recovered by the minimization algorithm. Thus the above formula applies for such a reconstructed signal's quality with $Var = 0$.

For nonzero variation the monotonicity again influences the signal quality. It is not possible to find a tight upper bound of the accumulated error, since the signal is recovered by the iterative minimization algorithm, for which no explicit solution exists.

However, in general, the recovered signal tends towards low frequency components. Thus, I assume that the maximum rate of change of the recovered signal is not larger than that of the original signal. Since the reconstructed signal has to be continuous when observed in a continuous time framework, on average, the recovered signal "slews" on at least:

$$x_{slew} = \frac{Var}{2 \cdot \max_i |\Delta x(i)|} \tag{47}$$

per measurement support group, where the geometric meaning of x_{slew} becomes clear from Fig. 8. This reduces the maximum possible error compared to the non-recovered signal, also indicated in fig. 8.
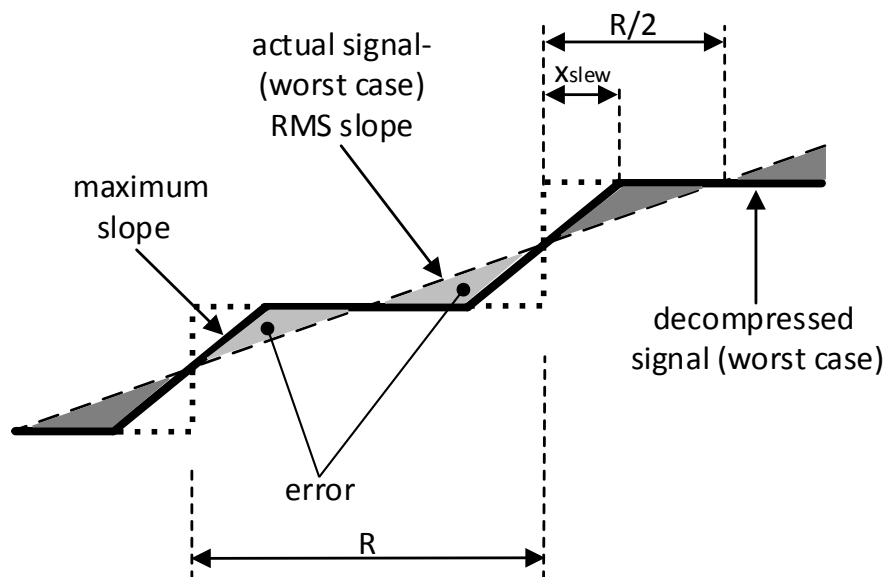

Fig. 8. Maximum difference among reconstructed and original signals with monotonic and largely variant measurement values

In this case, with $\beta = 0$, the maximum error is determined by:

$$\sum_{i=1+R(k-1)}^{R \cdot k} \left(x(i) - x'(i)\right)^2 \leq REC_{\beta 0} = 2 \int_0^{\frac{R}{2}-x_{slew}} \left(rms_i(\Delta\, x(i)) \cdot x\right)^2 dx$$

(48)

$$+2 \int_{\frac{R}{2}-x_{slew}}^{\frac{R}{2}} \left(rms_i(\Delta\, x(i)) \cdot x - \max_i|\Delta\, x(i)| \left(x - \frac{R}{2} + x_{slew}\right)\right)^2 dx$$

$$= 2\left(rms_i(\Delta\, x(i))\right)^2 \int_0^{\frac{R}{2}-x_{slew}} x^2 dx + 2\left(rms_i(\Delta\, x(i))\right)^2 \int_{\frac{R}{2}-x_{slew}}^{\frac{R}{2}} x^2 dx$$

$$- 4 \cdot rms_i(\Delta\, x(i)) \max_i|\Delta\, x(i)| \int_{\frac{R}{2}-x_{slew}}^{\frac{R}{2}} x\left(x - \frac{R}{2} + x_{slew}\right) dx$$

$$+ 2\left(\max_i|\Delta\, x(i)|\right)^2 \int_{\frac{R}{2}-x_{slew}}^{\frac{R}{2}} \left(x - \frac{R}{2} + x_{slew}\right)^2 dx$$

$$= \left(rms_i(\Delta\, x(i))\right)^2 \frac{R^3}{12} - 4 \cdot rms_i(\Delta\, x(i)) \cdot \max_i|\Delta\, x(i)| \left(\frac{R^3}{24} + \left(x_{slew} - \frac{R}{2}\right)\frac{R^2}{8} + \frac{\left(\frac{R}{2} - x_{slew}\right)^3}{6}\right)$$

$$+ 2\left(\max_i|\Delta\, x(i)|\right)^2 \left(\frac{R^3}{24} + \left(x_{slew} - \frac{R}{2}\right)\frac{R^2}{4} + \left(-\frac{R}{2} + x_{slew}\right)^2 \frac{R}{2} - \frac{\left(\frac{R}{2} - x_{slew}\right)^3}{3}\right).$$

The mean square error follows as:

$$MSE_{REC_{\beta 0}} = \frac{1}{R} \cdot \sum_{i=1+R(k-1)}^{R \cdot k} \left(x(i) - x'(i)\right)^2 = \frac{REC_{\beta 0}}{R}.$$
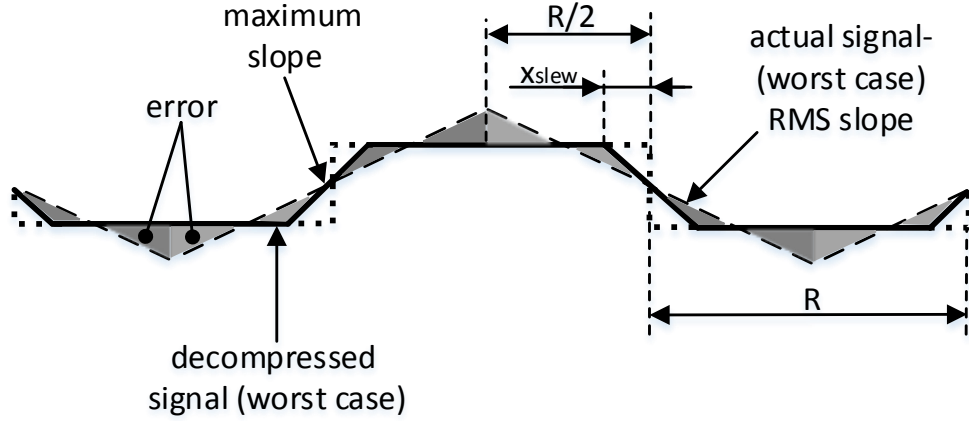
(49)

Fig. 9. Maximum difference among reconstructed and original signals with non-monotonic and largely variant measurement values

For maximum variation and $\beta = 1$ as shown in Fig. 9, the maximum error is determined by:

$$\sum_{i=1+R(k-1)}^{R \cdot k} \left(x(i) - x'(i)\right)^2 \leq REC_{\beta 1} = 4 \int_0^{\frac{R}{4} - x_{slew}} \left(\underset{i}{rms}\left(\Delta x(i)\right) \cdot x\right)^2 dx$$

(50)

$$+ 4 \int_{\frac{R}{4} - x_{slew}}^{\frac{R}{4}} \left(\underset{i}{rms}(\Delta x(i)) \cdot x - \underset{i}{max}|\Delta x(i)|\left(x - \frac{R}{4} + x_{slew}\right)\right)^2 dx$$

$$= 4 \left(\underset{i}{rms}(\Delta x(i))\right)^2 \int_0^{\frac{R}{4} - x_{slew}} x^2 dx + 4 \left(\underset{i}{rms}(\Delta x(i))\right)^2 \int_{\frac{R}{4} - x_{slew}}^{\frac{R}{4}} x^2 dx$$

$$- 8 \cdot \underset{i}{rms}(\Delta x(i)) \underset{i}{max}|\Delta x(i)| \int_{\frac{R}{4} - x_{slew}}^{\frac{R}{4}} x\left(x - \frac{R}{4} + x_{slew}\right) dx$$

$$+ 4 \left(\underset{i}{max}|\Delta x(i)|\right)^2 \int_{\frac{R}{4} - x_{slew}}^{\frac{R}{4}} \left(x - \frac{R}{4} + x_{slew}\right)^2 dx$$

$$= \left(\underset{i}{rms}(\Delta x(i))\right)^2 \frac{R^3}{48} - 8 \cdot \underset{i}{rms}(\Delta x(i)) \underset{i}{max}|\Delta x(i)| \left(\frac{R^3}{192} + \left(x_{slew} - \frac{R}{2}\right)\frac{R^2}{32} + \frac{\left(\frac{R}{4} - x_{slew}\right)^3}{6}\right)$$

$$+4\left(\max_i|\Delta\, x(i)|\right)^2\left(\frac{R^3}{192}+\left(x_{slew}-\frac{R}{4}\right)\frac{R^2}{16}+\left(x_{slew}-\frac{R}{4}\right)^2\frac{R}{4}-\frac{\left(\frac{R}{4}-x_{slew}\right)^3}{3}\right).$$

The accumulated squared error over all measurements and the mean square error

$MSE_{REC_{\beta 1}}=\frac{REC_{\beta 1}}{R}$ are determined the same way as above.

Table. 2. Mean Square Error as a function of Variation and

Monotonicity of the reconstructed signal

	$\beta = 0$	$\beta = 1$
$Var = 0$	$MSE = MSE_{MAX}$	$(MSE = MSE_{MAX})$
$Var = R\cdot\underset{i}{avg}(\Delta\, x(i))$	$MSE = MSE_{REC_{\beta 0}}$	$MSE = MSE_{REC_{\beta 1}}$

Thus incorporating a linear shift between the variations of MSE for the original vs.

recovered signal shapes as listed in Table 2 yields:

$$MSE = MSE_{MAX}+\frac{Var}{R\cdot\underset{i}{avg}(\Delta\, x(i))}\left((1-\beta)MSE_{REC_{\beta 0}}+\beta\cdot MSE_{REC_{\beta 1}}-MSE_{MAX}\right). \quad (51)$$

Then follows the PSNR of the reconstructed signal by:

$$(52)$$

$$PSNR(dB) = 10\cdot log\{S^2\}-10\cdot\log_{10}\{MSE_{MAX}$$

$$+\frac{Var}{R\cdot\underset{i}{avg}(\Delta\, x(i))}\left[(1-\beta)MSE_{REC_{\beta 0}}+\beta\cdot MSE_{REC_{\beta 1}}-MSE_{MAX}\right]\}$$

where MSE_{MAX}, $MSE_{REC_{\beta 0}}$ and $MSE_{REC_{\beta 1}}$ can be computed explicitly via (39), (49) and

(50) respectively.

EVALUATION OF THE DERIVED FRAMEWORK

In this section, computational results are provided to evaluate the PSNR expressions developed in the previous section. The parameters, if not varied to obtain a graph as a function of the given variable, are selected as follows:

- $N = 2500$ (Image with 2500 pixels, i.e., 50x50 pixel image)

- $S = 255$ (Standard image resolution of 8 bits)

- $C_{DC} = 7500$ (Average pixel strength of 150, value of DC component in Ψ equals $C_1 = N^{-\frac{1}{2}}$, and $C_{DC} = 150/C_1$. Note that this is because the AC components are centered at zero and do not contribute to the average signal strength.)

- $C_N = 5$ (Common value obtained from Matlab simulation results from a set of natural images)

- $P = 1\%$ (Coefficients whose magnitude is less than 1% of C_{DC} are considered to be insignificant)

- $\alpha = 0.7$ (From [6] follows that approximately 99% of all natural images have a coefficient α which is larger than 0.7)

- $N_{[s]}^* = 100$ ($N_{[s]}^*$ of the possible $N_{[s]}^{\max}$ coefficients in the low frequency window are dominant coefficients)

- $R = 6$

The parameters given above associated with the signal to be compressed are reasonable and represent practical data chosen from a set of natural images.

Fig. 10 depicts the achievable PSNR of the compressed signal computed via (46), as a function of the sparsity of the signal itself. Clearly, the less sparse the signal

(small α and large number of significant coefficients in the low frequency window), the

smaller the PSNR. If α is large, it is not critical if all low frequency coefficients are

significant. The graph shows however, that even very few dominant high frequency

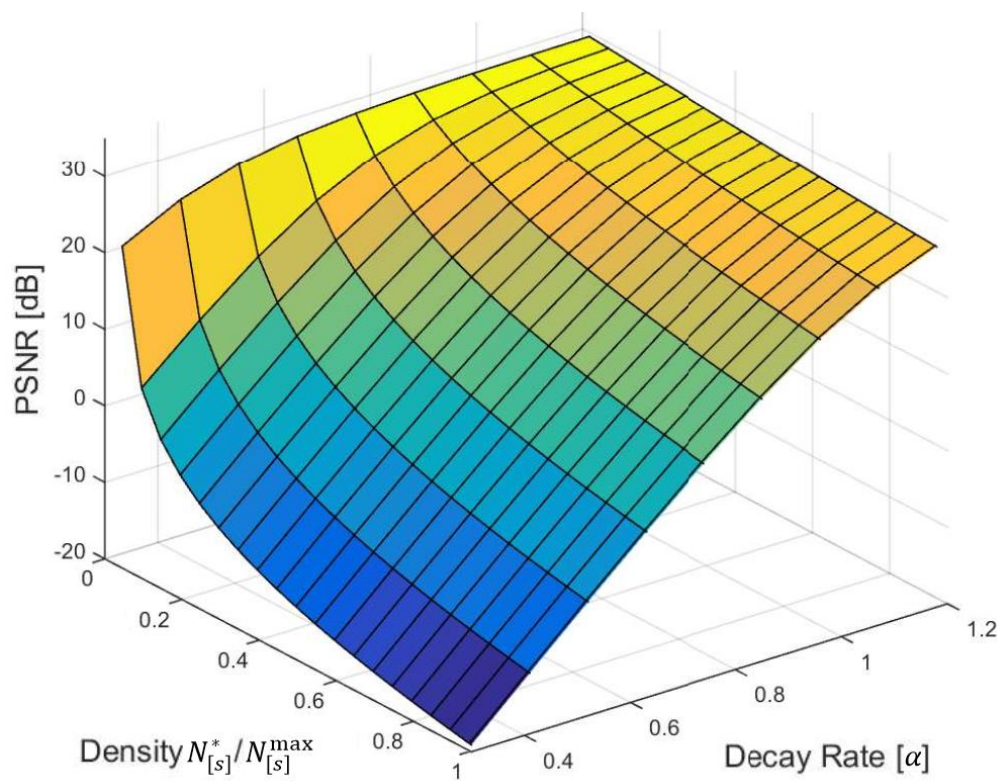coefficients dramatically limit the signal quality.

Fig. 10. Image quality as a function of number and location
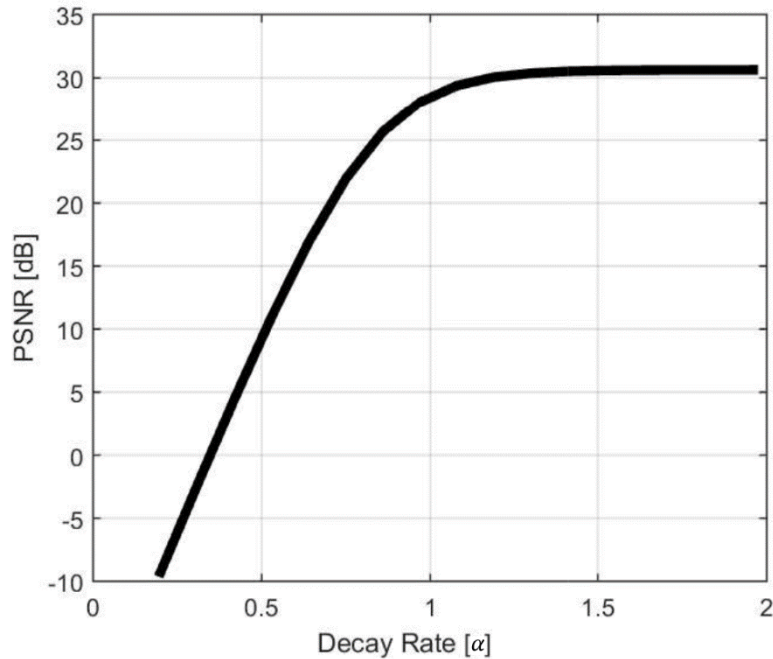of significant coefficients in $[s]_\Psi$

Fig. 11. Image quality with variable decay rate,
but constant number of significant coefficients

Fig. (11) shows the relation between decay rate α and the PSNR, with a constant number of dominant coefficients. Thus the same number of significant coefficients are distributed in variable size frequency windows, which are a function of α as given by (33). The steep slope of the graph, in the region with α smaller one, confirms that it is essential that dominant coefficients are contained in a tight window corresponding to low frequency bases vectors. Finally, Fig. 12 shows the effect of variable noise levels. The smaller high frequency noise, the better the proposed technique performs.
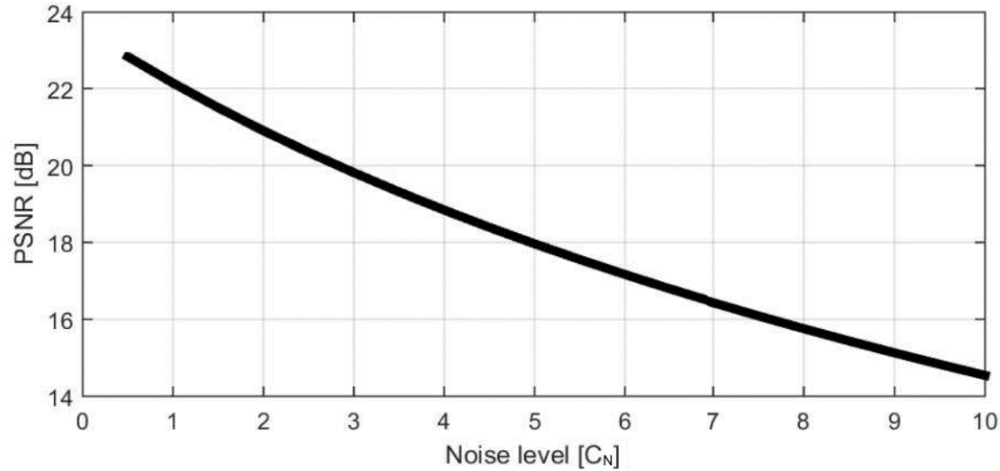
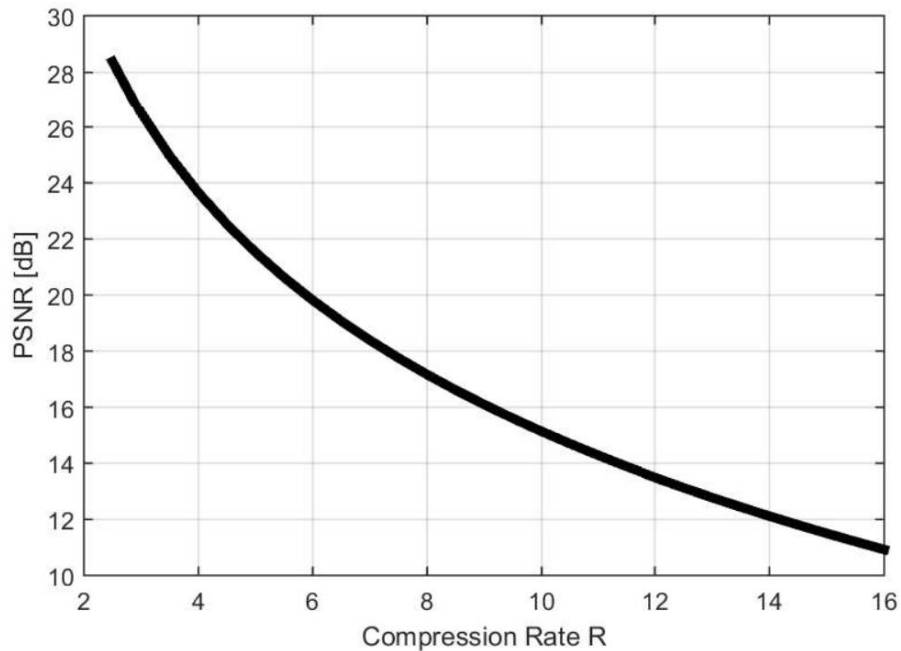Fig. 12. Image quality as a function of noise magnitude

Fig. 13. PSNR as a function of compression rate

Fig-s. 10, 11 and 12 demonstrate how the signal properties affect the compression technique. The result in Fig. 13 shows the effect of variable compression rate, which is controlled by the device performing the compression. As expected signal quality steadily drops as R increases. The graph shows PSNR values of about 23.7, 17.2 and 11 for compression rates of 4, 8 and 16 respectively. Thus doubling the compression rate

leads to a decrease in PSNR by approximately 6dB, which is equivalent to an increase

of MSE (45) by about a factor of four. The average sample value (strength of the signal)

is not performance critical. Thus varying C_{DC} has no significant impact on the results

presented above.

All simulation results presented above correspond to the compressed signal. The

equivalent computations for the reconstructed signals yield slightly higher results, but

not higher by several dB as expected. This is because the maximum slope computed in

(34) is very large. The model of the reconstructed signals as shown in fig-s. 8 and 9

may not be very realistic. In reality, on average, the slope of the signal section

connecting between two measurement supports must be much smaller than the

maximum possible slope, consequently leading to higher PSNR values. However, it is in

general very difficult to find an explicit upper bound for this average, as the

reconstructed solution is the output of an iterative minimization process. It will be part of

the future work to determine a more accurate measure and model for this case.

EXTENSION-LINEAR OBSERVATIONS IN TWO DIMENSIONS

The proposed measurement method in this section is to address degrading image quality when the compression rate increases, as observed in the results of fig.13. Forming linear observations with binary sparse matrices as presented in the proposed method section is very beneficial, when the compression rate is not very large. This is because the groups of samples where sums are formed are small, leaving not much freedom to relocate signal power compared to how it is distributed in the original signal. As R increases, these groups necessarily have to increase, leading to more signal power redistribution and consequently diminished quality of the reconstructed signal.
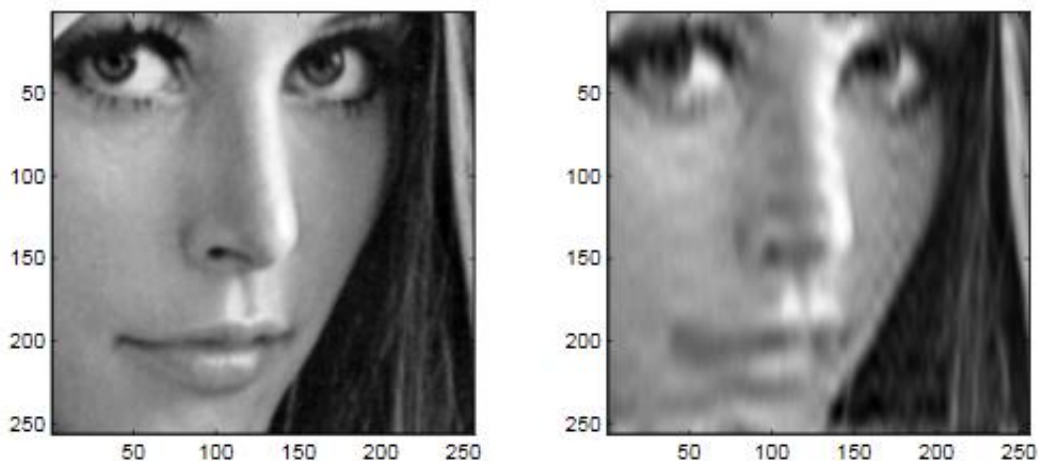

Fig. 14. Original (left) and compressed and reconstructed (right) Lenna image with a compression rate of 12

Simulation results of compressed and reconstructed images with compression rates of eight or higher show signal power redistribution following a clear pattern. The samples show oscillating behavior, as the reconstructed signal is the sparsest solution and thus is mainly represented by a small number of sinusoids. Therefore, the signal value changes from large to small and back to large steadily and consistently

throughout the whole frame, as clearly visible in Fig. 14. While this distribution satisfies the obtained linear observations (column wise or row wise), this significantly alters the power of the rows or columns of the 2D-signal respectively.

To address this negative effect, it should be very beneficial to perform measurements along columns and rows, and to combine the projections to form stiffer restrictions on the sparsest solution to be found. This way undesirable redistribution as shown above with oscillating signal power can be avoided. Incorporating this into [2] alters the minimization problem in the following way: Let x_h be the image data concatenated in a row by row fashion, and x_v the same in a column wise fashion. The sparse representations and the projections are given as:

$$x_h = \Psi \cdot [s_h]_\Psi \tag{53}$$

$$y_h = \Phi \cdot x_h \tag{54}$$

$$x_v = \Psi \cdot [s_v]_\Psi \tag{55}$$

$$y_v = \Phi \cdot x_v \tag{56}$$

Let T_{h-v} be the map which maps x_h to x_v. This map is uniquely defined and can be obtained by interchanging the rows of the n-dimensional identity matrix. Mathematically this relation yields:

$$x_v = T_{h-v} \cdot x_h \tag{57}$$

From (53), (55) and (57) follows that:

$$[s_v]_\Psi = \Psi^{-1} \cdot x_v = \Psi^{-1} \cdot T_{h-v} \cdot \Psi \cdot [s_h]_\Psi \tag{58}$$

Thus, the column and row wise projections can be expressed as a function of $[s_h]_\Psi$ by:

$$y_h = \Phi \cdot \Psi \cdot [s_h]_\Psi$$
$$y_v = \Phi \cdot \Psi \cdot [s_v]_\Psi = \Phi \cdot T_{h-v} \cdot \Psi \cdot [s_h]_\Psi \tag{59}$$

The minimization problem to solve for the sparsest solution satisfying all projections can then be modified to:

$$min\left|\left|[s_h]_\Psi\right|\right|_{l_1} \; subj.to \; \begin{bmatrix} y_h \\ y_v \end{bmatrix} = \begin{pmatrix} \Phi\Psi & O \\ O & \Phi T_{h-v}\Psi \end{pmatrix} \begin{bmatrix} [s_h]_\Psi \\ [s_h]_\Psi \end{bmatrix} \tag{60}$$

It is also possible to apply different measurement matrices to perform the column and row projections:

$$min\left|\left|[s_h]_\Psi\right|\right|_{l_1} \; subj.to \; \begin{bmatrix} y_h \\ y_v \end{bmatrix} = \begin{pmatrix} \Phi_h\Psi & O \\ O & \Phi_v T_{h-v}\Psi \end{pmatrix} \begin{bmatrix} [s_h]_\Psi \\ [s_h]_\Psi \end{bmatrix} \tag{61}$$

which enables different compression rates for the row and column measurements. To take advantage of this technique it is necessary to simultaneously reconstruct the pixel values of a rectangular array of samples, whereas in the conventional approach column independent reconstruction is possible. However, it has been observed by simulation that results improve with the size of the array of samples reconstructed simultaneously, such that this is not a disadvantage of this approach.

CONCLUSION AND FUTURE WORK

A new signal compression technique for signals with sparse, and low frequency representation has been introduced in this paper. Simulation results are provided to demonstrate the validity of the technique. Closed form expressions are developed to determine lower bounds for the quality of the compressed and reconstructed signals analytically. Comparing computed PSNR values and simulated data suggests that the framework to compute the compressed signal quality is valid, and provides insight into the dependence of signal quality on all parameters.

More work has to be done to predict achievable PSNR values in the reconstructed signal case. While the current lower bounds are valid, they are not very tight. Thus more accurate models, potentially involving statistical analysis, modeling the behavior of the minimization algorithm have to be developed. Also, in the current derivation, measurement matrices are assumed to add a small group of neighboring pixels, without overlap among measurement supports. Simulation suggests however that overlap is beneficial to achieve superb signal quality. While its benefit is intuitively clear, as it adds more constraints to the solution of the minimization algorithm, its effect has yet to be understood and described analytically.

REFERENCES

1. "Image Sensor Market by Technology (CMOS, CCD), Spectrum, Array, Scanning Method, Application (Consumer Electronics, Healthcare, Industrial, Security, Automotive, Aerospace, and Defense) and by Geography - Analysis and Forecast (2013 - 2020)," http://www.marketsandmarkets. com/MarketImage-Sensor-Semiconductor-Market-601.html

2. Tang, F., Chen, D. G., Wang, B., and Bermak, A., "Low-Power CMOS Image Sensor Based on Column-Parallel Single-Slope/SAR Quantization Scheme," IEEE Transactions on Electron Devices, vol.60, no.8, pp.2561,2566, Aug. 2013

3. Gao, Q., and Yadid-Pecht, O., "A Low-Power Block-Based CMOS Image Sensor With Dual VDD," IEEE Sensors Journal, vol.12, no.4, pp.747,755, April 2012

4. Donoho, D. L., "Compressed sensing," IEEE Transactions on Information Theory, vol. 52, no. 4, 2006, pp.1289–1306

5. Candès, E. J., Romberg, J. K., and Tao, T., "Stable signal recovery from incomplete and inaccurate measurements," Communications on Pure and Applied Mathematics, vol. 59, no. 8, 2006, pp. 1207–1223

6. A. Torralba and A. Oliva, "Statistics of Natural Image Categories," Network: Computation in Neural Systems, vol. 14, no. 3, 2003, pp. 391–412, 2003

7. Candes, E. J., and Wakin, M. B., "An Introduction To Compressive Sampling," IEEE Signal Processing Magazine, vol. 25, no.2, 2008, pp.21-30

8. Berinde, R., Gilbert, A. C., Indyk, P., Karloff, H., and Strauss, M. J., "Combining geometry and combinatorics: A unified approach to sparse signal recovery,"

Communication, Control, and Computing, 2008 46th Annual Allerton Conference on, Urbana-Champaign, IL, 2008, pp. 798-805

9. Q. Huynh-Thu and M. Ghanbari, "Scope of validity of PSNR in image/video quality assessment," in Electronics Letters, vol. 44, no. 13, 2008, pp. 800-801

10. S. Leitner, H. Wang and S. Tragoudas, "Compressive Image Sensor Technique with Sparse Measurement Matrix," 2016 29th IEEE International System-on-Chip Conference (SOCC), Seattle, 2016

11. N. Kulkarni, P. Nagesh, R. Gowda and B. Li, "Understanding Compressive Sensing and Sparse Representation-Based Super-Resolution," in *IEEE Transactions on Circuits and Systems for Video Technology*, vol. 22, no. 5, pp. 778-789, May 2012

VITA

Graduate School
Southern Illinois University

Stefan Leitner

ls3130@siu.edu

Management Center Innsbruck
Bachelor of Science, Mechatronics- Machinery Construction, July 2013

Southern Illinois University
Master of Science, Electrical & Computer Engineering, December 2016

Research Paper Title:
    Underdetermined Signal Representation via Linear Projections using Binary
    Sparse Matrices- Signal Compression

Major Professor: Dr. Kathleen Pericak Spector

Publications:
    S. Leitner, H. Wang and S. Tragoudas, "Design Techniques for Direct Digital Synthesis Circuits with Improved Frequency Accuracy over Wide Frequency Ranges," Journal of Circuits, Systems, and Computers
    S. Leitner and H. Wang, "Current compensation techniques for low-voltage high-performance current mirror circuits," Journal of Analog Integrated Circuits and Signal Processing, vol. 88, no. 1, pp.79-88, 2016
    S. Leitner, H. Wang and S. Tragoudas, "Compressive Image Sensor Technique with Sparse Measurement Matrix," 2016 29th IEEE International System-on-Chip Conference (SOCC), Seattle, 2016
Nominated for Best paper Award
    S. Leitner, P. West, C. Lu and H. Wang, "Digital LDO Modeling for Early   Design Space Exploration," 2016 29th IEEE International System-on-Chip Conference (SOCC), Seattle, 2016
Nominated for Best paper Award
    S. Koyada, A. K. Nagabhushana, S. Leitner and H. Wang, "An A-SAR ADC circuit with adaptive auxiliary comparison scheme," 2015 8th IEEE International System-on-Chip Conference (SOCC), Beijing, 2015, pp. 197-202